Dynamic action potential clamp predicts functional separation in mild familial and severe de novo forms of *SCN2A* epilepsy

Géza Berecki[a,1], Katherine B. Howell[b,c,d], Yadeesha H. Deerasooriya[e], Maria Roberta Cilio[f,g], Megan K. Oliva[a], David Kaplan[a], Ingrid E. Scheffer[a,b,c,h], Samuel F. Berkovic[h], and Steven Petrou[a,i,j,k,1]

[a]Ion Channels and Disease Group, The Florey Institute of Neuroscience and Mental Health, University of Melbourne, Parkville, VIC 3052, Australia; [b]Department of Neurology, Royal Children's Hospital, Parkville, VIC 3052, Australia; [c]Department of Pediatrics, University of Melbourne, Parkville, VIC 3052, Australia; [d]Murdoch Children's Research Institute, Parkville, VIC 3052, Australia; [e]Department of Mechanical Engineering, University of Melbourne, Parkville, VIC 3052, Australia; [f]Department of Neurology, University of California, San Francisco Benioff Children's Hospital, University of California, San Francisco, CA 94158; [g]Department of Pediatrics, University of California, San Francisco Benioff Children's Hospital, University of California, San Francisco, CA 94158; [h]Epilepsy Research Centre, Department of Medicine, University of Melbourne, Austin Health, Heidelberg, VIC 3084, Australia; [i]Department of Medicine, Royal Melbourne Hospital, University of Melbourne, Parkville, VIC 3050, Australia; [j]Australian Research Council (ARC) Centre of Excellence for Integrated Brain Function, University of Melbourne, Parkville, VIC 3052, Australia; and [k]RogCon, Inc., Cambridge, MA 02142

Edited by Bruce P. Bean, Harvard Medical School, Boston, MA, and approved May 9, 2018 (received for review January 3, 2018)

De novo variants in *SCN2A* developmental and epileptic encephalopathy (DEE) show distinctive genotype–phenotype correlations. The two most recurrent *SCN2A* variants in DEE, R1882Q and R853Q, are associated with different ages and seizure types at onset. R1882Q presents on day 1 of life with focal seizures, while infantile spasms is the dominant seizure type seen in R853Q cases, presenting at a median age of 8 months. Voltage clamp, which characterizes the functional properties of ion channels, predicted gain-of-function for R1882Q and loss-of-function for R853Q. Dynamic action potential clamp, that we implement here as a method for modeling neurophysiological consequences of a given epilepsy variant, predicted that the R1882Q variant would cause a dramatic increase in firing, whereas the R853Q variant would cause a marked reduction in action potential firing. Dynamic clamp was also able to functionally separate the L1563V variant, seen in benign familial neonatal–infantile seizures from R1882Q, seen in DEE, suggesting a diagnostic potential for this type of analysis. Overall, the study shows a strong correlation between clinical phenotype, *SCN2A* genotype, and functional modeling. Dynamic clamp is well positioned to impact our understanding of pathomechanisms and for development of disease mechanism-targeted therapies in genetic epilepsy.

de novo SCN2A mutation | dynamic action potential clamp | epilepsy | voltage clamp | modeling

Mutations in *SCN2A*, encoding the voltage-gated sodium channel type IIα subunit ($Na_v1.2$), cause familial and sporadic brain disorders. Familial mutations were first identified in self-limited, pharmacoresponsive epilepsy typically arising from gain-of-function mutations (1), whereas de novo mutations were only more recently discovered and have been recognized as the most frequent cause of neurodevelopmental disorder (2–7). The phenotypic spectrum of *SCN2A* mutations is broad, ranging from age-limited, pharmacoresponsive epilepsy with normal development, to severe conditions with refractory epilepsy and severe developmental impairment, known as developmental and epileptic encephalopathies (DEE) (1, 8–11). DEEs are a group of brain disorders with impairment of neurodevelopment where epileptic activity per se adds to the neurodevelopmental impairment (12).

Within the DEEs, distinct phenotypes are emerging among individuals with *SCN2A* variation (7, 10). Particularly, there is a group of patients with seizure onset in the early infantile period ("early-onset") in whom sodium-channel blockers, such as phenytoin and carbamazepine, may improve seizures, and a group with seizure onset later in infancy ("later-onset" group, >3 mo) in whom sodium-channel blockers are rarely effective (2, 7). It has been postulated that the difference in clinical features and treatment response are due to differential effects of the *SCN2A* mutations on $Na_v1.2$ channel function (7). De novo *SCN2A* variants exhibiting $Na_v1.2$ channel gain-of-function are typically associated with epilepsy, whereas it has been proposed that partial

Significance

***SCN2A*, encoding the voltage-gated sodium channel $Na_v1.2$, has emerged as a major gene implicated in neonatal-, infantile-, and even childhood-onset epilepsies. Many of these epilepsies are also associated with cognitive and behavioral impairments that range in type and severity. The biophysical, neurophysiological, and clinical impacts of *SCN2A* mutations are poorly understood. Here, we use clinical evaluation and biophysical analyses to explore the mechanisms underpinning distinctive phenotypes produced by *SCN2A* variants associated with mild familial or severe de novo forms of epilepsy. We show that dynamic clamp analysis provides clear benefits over conventional voltage clamp for a rapid and definitive prediction of neuron-scale phenotypic consequences, and is well positioned to impact diagnosis and drug discovery in genetic epilepsy.**

Author contributions: G.B. and S.P. designed research; G.B. performed research; Y.H.D., M.K.O., D.K., S.F.B., and S.P. contributed new reagents/analytic tools; G.B., K.B.H., Y.H.D., M.R.C., and I.E.S. analyzed data; G.B., K.B.H., and S.P. wrote the paper; K.B.H., M.R.C., and I.E.S. collected and summarized electro-clinical data; and Y.H.D. contributed to the editing of the paper.

Conflict of interest statement: G.B. is funded by RogCon, Inc., Miami, Florida, a biotechnology company focused on drug research, discovery, and development for select ion channelopathies, including SCN2A. I.E.S. has served on scientific advisory boards for UCB, Eisai, GlaxoSmithKline, Biomarin, and Nutricia; editorial boards of the *Annals of Neurology*, *Neurology and Epileptic Disorders*; may accrue future revenue on pending patent WO61/010176 (filed: 2008): Therapeutic Compound; has received speaker honoraria from GlaxoSmithKline, Athena Diagnostics, UCB, Eisai, and Transgenomics; has received funding for travel from Athena Diagnostics, UCB, Biocodex, GlaxoSmithKline, Biomarin, and Eisai; and receives/has received research support from the National Health and Medical Research Council of Australia, National Institutes of Health, Australian Research Council, Health Research Council of New Zealand, CURE, The American Epilepsy Society, the US Department of Defense Autism Spectrum Disorder Research Program, March of Dimes, and Perpetual Charitable Trustees. S.P. is cofounder, Chief Scientific Officer, and equity holder of RogCon, Inc., Miami, Florida, a biotech company focused on the delivery of novel therapeutics for SCN2A disorders. RogCon, Inc. provided funding for this project. S.P. is also cofounder and equity holder in Praxis Precision Medicines, Inc., Cambridge, Massachusetts, which develops precision medicines for neurogenetic disorders, including those caused by SCN2A mutations. S.P. is a Scientific Advisor and equity holder in Pairnomix, Inc., Minneapolis, Minnisota, which is undertaking precision medicine development in epilepsy and related disorders.

This article is a PNAS Direct Submission.

[1]To whom correspondence may be addressed. Email: geza.berecki@florey.edu.au or steve.petrou@unimelb.edu.au.

This article contains supporting information online at www.pnas.org/lookup/suppl/doi:10.1073/pnas.1800077115/-/DCSupplemental.

Published online May 29, 2018.

or complete $Na_v1.2$ channel loss-of-function would invariably lead to autism spectrum disorder (10). However, more recently, loss-of-function has been also associated with later-onset epilepsy, suggesting the genotype–phenotype correlation may be more complex (7).

Therefore, there is an urgent need for a comprehensive understanding of the biophysical, neurophysiological, and clinical impacts of different mutation classes for diagnosis and for the development of disease mechanism-based therapies. Here, we undertake a detailed functional analysis of two of the most recurrent *SCN2A* variants, R1882Q and R853Q. We present a comprehensive clinical evaluation for all R1882Q and R853Q cases where records or literature data were available. In addition, we implement dynamic action potential-clamp analysis to the study of *SCN2A* variants in epilepsy and show how this approach has the potential to provide a rapid and definitive prediction of neuron scale phenotypic consequences.

Functional studies of $Na_v1.2$ channel variants in mammalian cells or *Xenopus* oocytes using patch-electrode and two-electrode voltage clamp, respectively, represent the current gold standard for analysis of *SCN2A* and other voltage-gated ion channels in epilepsy. Both these methods are able to dissect various functional states of ion channel behavior, typically including voltage dependence and kinetics of various transitions from open to inactivated and the reversal or recovery of these states. Often, functional analysis is followed by an intuitive interpretation to predict whether a particular change in a biophysical character would enhance or diminish the activity in the neuron in which a particular ion channel resides. This can lead to various interpretations of enhanced excitability in pyramidal neurons or disinhibition in interneurons that are credited with being the underlying cause of a particular epilepsy syndrome. More formal but time-consuming post hoc computational analysis of the biophysical properties of a given channel can be carried out to remove the perils of intuition and the bias of interpretation, but these are rarely undertaken.

The recently developed dynamic action potential-clamp methodology can bridge the divide from intuition to formal modeling (13, 14) and can enable rapid and unambiguous determination of the effects of ion channel mutations on neuronal excitability without the need for time-demanding voltage clamp characterization. This method produces a real-time coupling between a biological cell and an in silico cell to generate a hybrid neuron model that predicts the impact of ion channel variation on neuronal excitability. Unlike traditional post hoc modeling, there is no need to comprehensively characterize the underlying biophysics of the channel of interest. By using a variety of in silico models it is possible to gauge the impact of a variant in different neuronal compartments, such as soma, axon initial segment or dendrite, or even different neuronal types, such as interneuron or cortical layer-specific pyramidal neuron to provide different contexts for interpreting disease mechanisms.

Here, we deploy the dynamic action potential-clamp approach to analyze the impacts of the R853Q and R1882Q DEE variants, as well as the L1563V variant previously associated with inherited benign familial neonatal infantile seizures (BFNIS) (15–17). R853Q and R1882Q are the most frequently identified *SCN2A* variants and are associated with specific phenotypes. We not only show how successfully dynamic action potential-clamp analysis can recapitulate and surpass voltage clamp findings, but also demonstrate how it can be superior to intuitive interpretation when faced with biophysical changes that have opposing effects on excitability. Our dynamic action potential clamp data directly demonstrate that the early-onset R1882Q DEE variant results in increased neuronal excitability and that the late-onset R853Q DEE variant results in decreased neuronal excitability. Voltage clamp analysis of the L1563V variant associated with self-limited and pharmacoresponsive BFNIS resulted in opposing changes in voltage dependence of activation and inactivation with enhanced recovery from fast inactivation whose impact on excitability would be difficult to interpret. Dynamic action potential clamp could clearly predict how these opposing changes could result in an enhanced excitability profile and how this could be separated from the functional profile of the more-severe R1882Q variant. Dynamic action potential clamp is well positioned to impact diagnosis and drug discovery in genetic epilepsy and is particularly relevant in the current era of precision medicine.

Results

Patients with *SCN2A* Mutations. Seven individuals with the R1882Q and 12 with the R853Q recurrent mutations were identified. Distinct phenotypic features, particularly age of seizure onset and initial seizure type, applied to the patient groups with R1882 or R853Q mutations (Table1). Sodium-channel blockers were mainly beneficial in the R1882Q group. Movement disorders occurred in both groups; however, severe choreoathetosis only occurred with the R853Q mutation. The cellular and network pathophysiological mechanisms leading to movement disorders in these patients are unknown.

A summary of clinical features and treatment response of individual patients is shown in *SI Appendix*. We previously reported the phenotypic data for the patients with the familial L1563V BFNIS mutation (1).

Table 1. General clinical features and treatment response of patients with epilepsy and/or developmental delay

Phenotypic group	Age seizure onset	Onset seizure type	Seizures improve with PHT?	Seizures improve with other Na_v channel blockers?	Other seizure types later	Ongoing seizures after infancy?	Movement disorder/ paroxysmal neurological symptoms	Developmental delay (±autism)
Benign epilepsy (BFNIS) (e.g., L1563V)	0–13 mo	Focal	Unknown	Unknown	No	No	No	No
Severe epilepsy								
Early-onset (e.g., R1882Q)								
Intermediate	0–3 mo	Focal	Variable (marked benefit some)	Variable (may improve)	No	Variable	Variable	Variable (normal-mod. DD)
Severe					Variable	Yes	Yes	Yes (severe-profound DD)
Late-onset (e.g., R853Q)	>3 mo	Spasms	No (may worsen)	Variable (reports of both benefit and worsening)	Yes	Yes	Yes (may predate Sz)	Yes (moderate-severe DD, DD predates Sz)

DD, developmental delay; PHT, phenytoin; Sz, seizures.

Biophysical Characterization of $Na_v1.2$ Channel Variants Using Conventional Voltage Clamp. To understand the basis of clinical heterogeneity in *SCN2A*-associated disorders, the biophysical consequences of $Na_v1.2$ channel mutations and their impact on action potential firing and neuronal excitability must be clarified. Representative current traces from Chinese hamster ovary (CHO) cells transiently expressing wild-type or mutant $Na_v1.2$ channels are shown in Fig. 1*B*. Peak sodium current (I_{Na}) densities in cells expressing L1563V channels were similar to those of wild-type channels, whereas I_{Na} densities were decreased in cells harboring R853Q channels and increased in cells harboring R1882Q channels (Fig. 1*C* and Table 2). The effects of mutations on $Na_v1.2$ channel gating over a range of membrane potential (V_m) values are shown in Fig. 1*D*. Relative to wild-type, the activation curves of R853Q and L1563V channels exhibited small but statistically significant hyperpolarizing or depolarizing shifts, respectively. R1882Q channel activation was more severely affected, resulting in a 6-mV hyperpolarizing shift of the $V_{0.5,act}$ value, a change that results in increased sodium-channel availability compared with the wild-type (Fig. 1*D* and Table 2). In all mutants, the $V_{0.5,inact}$ values were significantly changed compared with wild-type (Fig. 1*D* and Table 2). In cells expressing R853Q channels, the hyperpolarizing shift of $V_{0.5,inact}$ stabilizes inactivation and leads to reduced sodium-channel availability at physiologically relevant V_m values. Conversely, the depolarizing shift of $V_{0.5,inact}$ increases sodium-channel availability for L1563V and R1882Q variants.

The overlapping regions of the I_{Na} activation and inactivation curves (Fig. 1*D*) suggested the presence of a "window current" arising from partial activation and incomplete inactivation of the $Na_v1.2$ channel. Inward window current is capable of contributing to depolarization even at resting potentials (18). We determined the voltage dependence of the quasi steady-state open probability (P_o) (19) of the wild-type and mutant channels (Fig. 2*A*). The peak of the P_o distribution of R1882Q channels was markedly greater than that seen in wild-type, whereas the peak of the P_o distribution of L1563V was only modestly greater than wild-type. In contrast, R853Q channels showed a significant reduction in the peak of the P_o distribution (Fig. 2*A* and Table 2). The areas under the P_o distribution for each variant were used to estimate the overall contribution of window current to the total I_{Na} (Fig. 2*A* and Table 2). Compared with wild-type, this value decreased for R853Q channels and showed moderate or large increase for L1563V or R1882Q channels, respectively. For R853Q channels we also hypothesized that replacement of the positively charged arginine in the voltage sensor with the neutral amino acid glutamine could result in gating pore current (20). However, we were unable to demonstrate the presence of pore currents in cells expressing R853Q channels (*SI Appendix*, Fig.

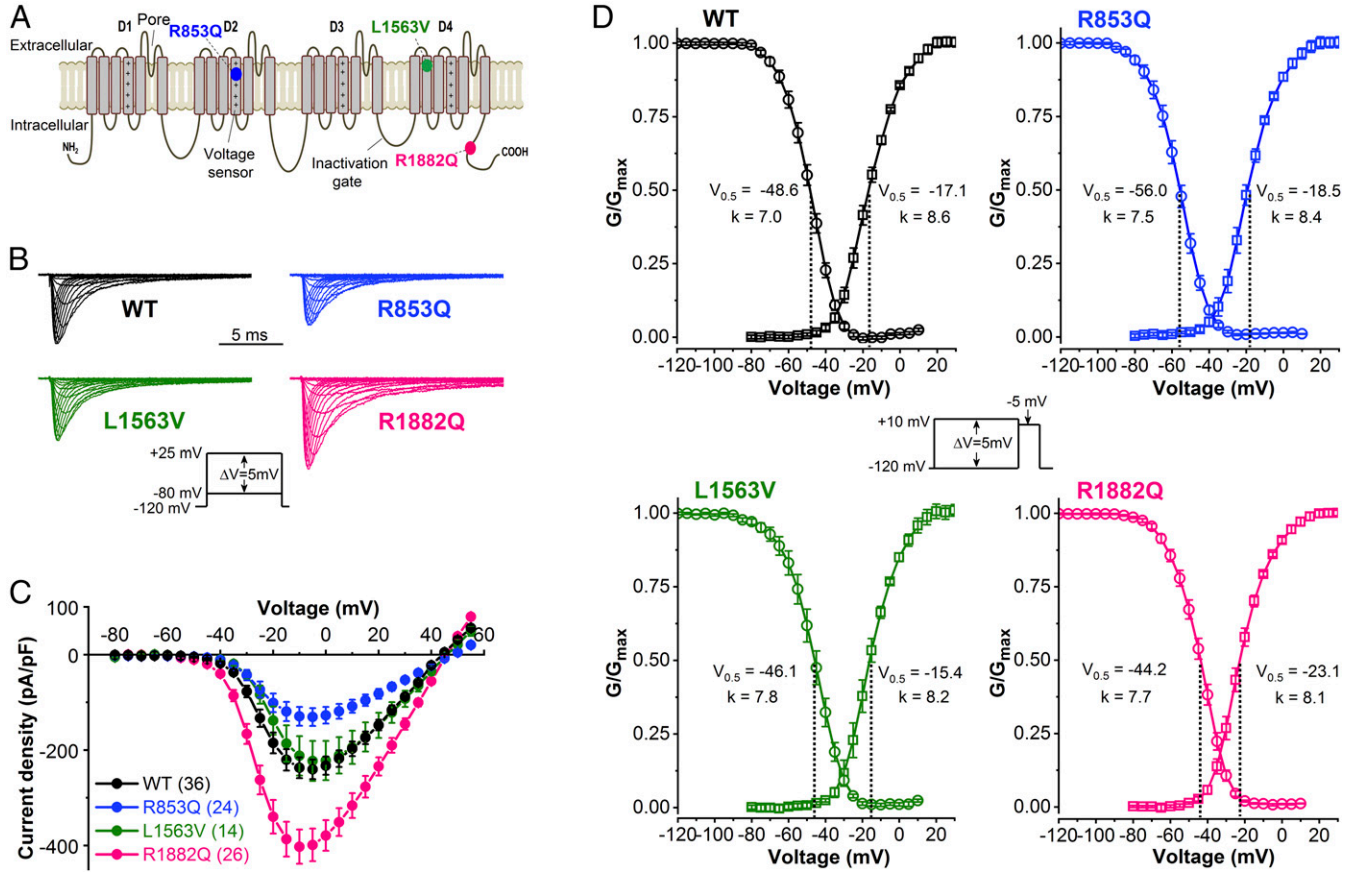

Fig. 1. Location of $Na_v1.2$ mutations and biophysical properties of wild-type (WT), R853Q, L1563V, and R1882Q channels. (*A*) Predicted transmembrane topology of $Na_v1.2$ channels denoting the R853Q and R1882Q mutations associated with later-onset and early-onset DEE respectively, and the L1563V mutation associated with BFNIS. Domains D1–D4 are indicated; note the positive charges on the voltage sensor (fourth segment) of each domain. (*B*) Representative wild-type and mutant I_{Na} traces, elicited by 20-ms depolarizing voltage steps of 5-mV increment from a HP of −120 mV (*Inset* voltage protocol). (*C*) Current–voltage relationships. (*D*) Voltage dependence of activation (squares) and inactivation (circles). The normalized conductance–voltage relationships are plotted as G/G_{max} values versus voltage and are referred to as "activation" curves. Curves were obtained by nonlinear least-squares fits of Boltzmann equations (*Materials and Methods*). Values of fitted parameters are indicated below each curve and summarized in Table 2. Activation was assessed using the voltage protocol described in *B*. Inactivation was determined from a HP of −120 mV using 100-ms conditioning steps ranging from −120 to +10 mV followed by 20-ms test pulses to −5 mV (*Inset*), at 0.1 Hz. The number of experiments, *n*, are shown in Table 2.

Table 2. Biophysical parameters of I_{Na} through $Na_v1.2$ channel variants

Biophysical property	Wild-type	R853Q	L1563V	R1882Q
Current density, pA/pF	240.4 ± 21	130.7 ± 19*	222.7 ± 42	402.0 ± 36****
n	36	24	14	26
Activation				
$V_{0.5,act}$, mV	−17.06 ± 0.25	−18.49 ± 0.31***	−15.39 ± 0.29***	−23.08 ± 0.26****
k_{act}, mV	8.63 ± 0.25	8.44 ± 0.28	8.19 ± 0.26	8.09 ± 0.26
n	36	24	14	26
Inactivation				
$V_{0.5,inact}$, mV	−48.60 ± 0.24	−55.98 ± 0.69****	−46.08 ± 0.49***	−44.23 ± 0.26****
k_{inact}, mV	7.00 ± 0.21	7.45 ± 0.35	7.83 ± 0.44	7.67 ± 0.24
n	31	21	14	25
Open probability, P_o				
$m \times h$	0.012 ± 4e^{-5}	0.0078 ± 3e^{-5}****	0.016 ± 4e^{-5}****	0.036 ± 2e^{-4}****
x_c, mV	−38.7 ± 0.1	−41.0 ± 0.2****	−30.1 ± 0.1****	−34.0 ± 0.2****
w_1, mV	14.9 ± 0.1	16.9 ± 0.2****	16.4 ± 0.1****	14.43 ± 0.2
w_2, mV	16.9 ± 0.1	18.5 ± 0.2****	16.19 ± 0.1*	14.53 ± 0.2****
Window I_{Na}				
Area, % of total	1.1 ± 0.06	0.91 ± 0.05*	1.35 ± 0.09*	2.1 ± 0.14**
Persistent I_{Na}				
At −30 mV, % of total	1.18 ± 0.13	1.24 ± 0.14	1.23 ± 0.22	2.92 ± 0.25****
n	30	21	14	25
Time course of fast inactivation				
τ_f at −30 mV, ms	2.43 ± 0.20	2.23 ± 0.25	2.47 ± 0.24	3.26 ± 0.22**
n	20	14	11	20
Time course of recovery†				
τ at −120 mV, ms	0.90 ± 0.06	0.93 ± 0.09	0.51 ± 0.07****	0.92 ± 0.06
τ at −70 mV, ms	8.22 ± 0.3	8.29 ± 0.5	3.47 ± 0.2****	8.35 ± 0.5
n	16	14	10	15
Slow inactivated I_{Na} fraction				
After 195, at −60 mV	0.23 ± 0.02	0.33 ± 0.02**	0.16 ± 0.02*	0.21 ± 0.02
After 195, at −50 mV	0.62 ± 0.02	0.71 ± 0.02**	0.51 ± 0.02***	0.61 ± 0.02
n	12	9	9	8
Time course of slow inactivation				
τ_f at −60 mV, ms	677.5 ± 28	310.6 ± 18	5,279 ± 480****	1,508 ± 144
τ_f at −50 mV, ms	777.0 ± 36	650 ± 43	2,443 ± 207****	1,240 ± 111*
τ_s at −60 mV, s	70.0 ± 11.1	78.0 ± 8.4	84.4 ± 19.6	68.6 ± 6.2
τ_s at −50 mV, s	46.6 ± 6.5	47.6 ± 7.7	52.4 ± 6.5	47.2 ± 5.6
n	12	9	9	8

Data are represented as mean ± SEM; *h*, probability that a channel is not inactivated; $k_{(in)act}$, slope factor of steady-state (in)activation curve; *m*, probability that the channel is activated; *n*, number of cells measured; $V_{0.5,(in)act}$, membrane potential for half-maximal (in)activation. *A* represents the peak of the P_o curve, x_c is the voltage below the peak, w_1 and w_2 represent width for *m* and *h*, respectively. τ_f and τ_s, fast and slow time constants, respectively; *$P < 0.05$, **$P < 0.01$, ***$P < 0.001$, or ****$P < 0.0001$ compared with wild-type, one-way ANOVA with Bonferroni correction.

†Recovery from fast inactivation.

S1), suggesting that pore currents do not contribute to the pathophysiological mechanism in these cells.

In cells expressing R1882Q channels, the analysis of I_{Na} during depolarization revealed a slower time course of inactivation compared with wild-type channels and the presence of a non-inactivating persistent inward I_{Na} that was nearly absent in cells expressing wild-type channels (Fig. 2*B*). The persistent I_{Na} was sensitive to 100 nM tetrodotoxin, indicating that this current component was mediated by the transfected $Na_v1.2$ channels and not an endogenous current. In cells expressing R853Q and L1563V channels, the magnitude of persistent I_{Na} was similar to that of wild-type channels (Fig. 2*B* and Table 2). In the voltage range between −40 mV and +10 mV, the time constants of peak I_{Na} inactivation of R853Q and L1563V channels were unchanged compared with wild-type, whereas R1882Q channels exhibited impaired fast inactivation (Fig. 2*C* and Table 2).

Next, we studied the kinetic features of recovery and slow inactivation of wild-type and mutant $Na_v1.2$ channels. Recovery from inactivation in sodium channels is a time- and voltage-dependent process following action potentials or depolarizing voltage steps (21, 22). For example, as shown in Fig. 3*A*, wild-type or variants channel recovery was around 10 times more rapid at −120 mV compared with −70 mV. Interestingly, only the L1563V variant showed a significantly more rapid recovery than wild-type channels, consistent with a gain-of-function effect. In contrast, the time constants of recovery for R853Q and R1882Q channels were similar to that of wild-type (Fig. 3*A* and Table 2). We evaluated the entry of wild-type and variant channels into slow inactivation. Both the time course and the extent of slow inactivation were enhanced at more depolarizing potentials (Fig. 3*B*), consistent with earlier studies (23). At two different test voltages, R1882Q channels entered slow inactivation similarly to wild-type channels, whereas L1563V showed reduced entry and R853Q showed enhanced entry (Fig. 3*B* and Table 2).

Dynamic Action Potential-Clamp Studies of Epileptogenic $Na_v1.2$ Channels. In dynamic clamp mode (Fig. 4*A*), we characterized the voltage responses of the hybrid cell model incorporating wild-type or mutant (R853Q, L1563V, or R1882) I_{Na} expressed in CHO cells, and leak and delayed rectifier currents represented solely in the in silico model. We used two stimulating protocols to elicit action potentials. First, we used current steps of 500- or

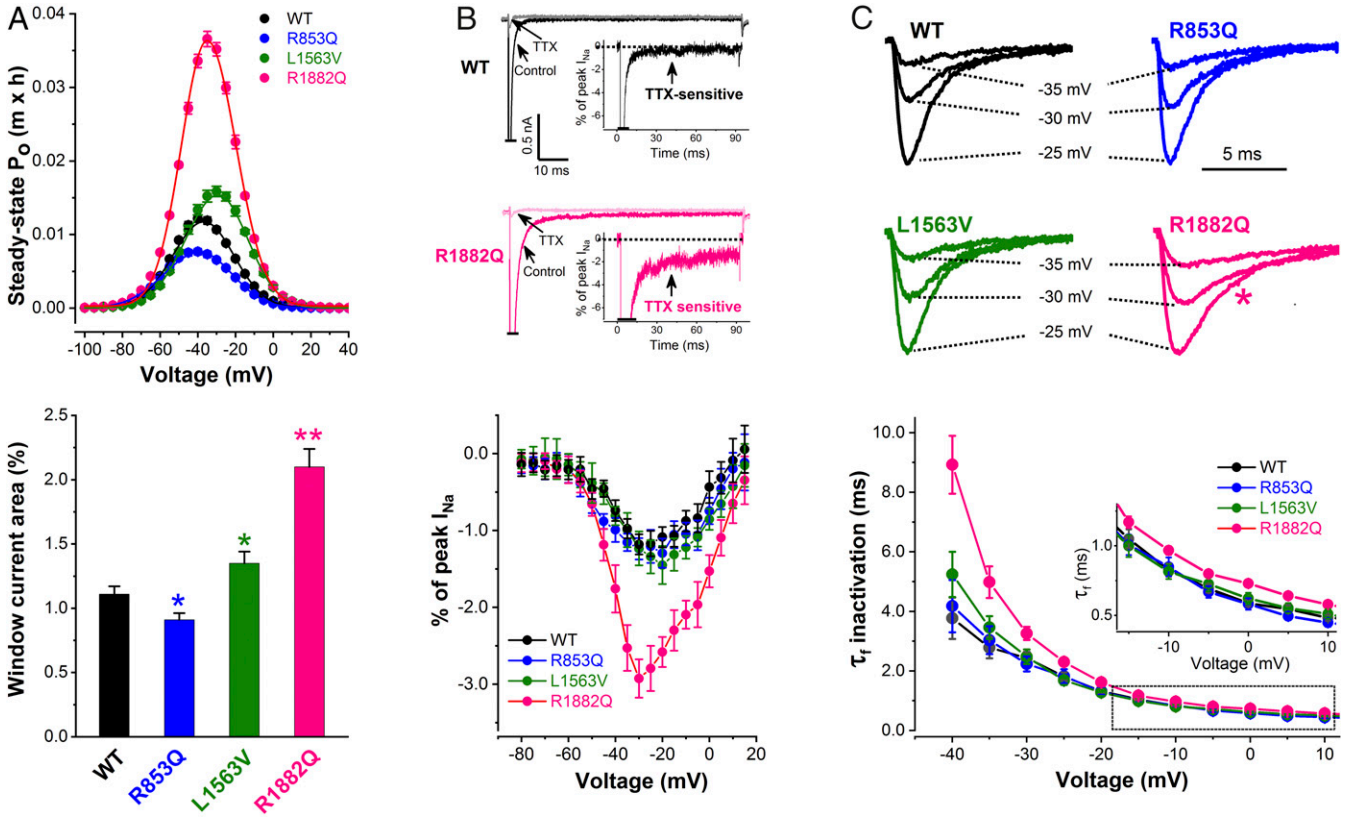

Fig. 2. Mechanisms contributing to sodium channel dysfunction in R853Q, L1563V, and R1882Q channels. (*A*) Voltage dependence of the steady-state open probability (P_o) (*Upper*). The $m \times h$ product was calculated for every cell using the individual G/G_{max} values described in Fig. 1*D*, and plotted against the V_m. (*Lower*) Mean percentages of window current relative to total current in wild-type (WT) and mutant $Na_v1.2$ channels. Data are represented as mean ± SEM (*n*, same as in Fig. 1*D*) (see data with statistics in Table 2). $*P < 0.05$, $**P < 0.01$. (*B*) Demonstration of persistent inward I_{Na}. (*Upper*) Sensitivity of persistent inward I_{Na} to tetrodotoxin (TTX). Peak currents are off scale. *Insets* show TTX sensitive current as percentage of peak I_{Na}, obtained by subtraction. (*Lower*) Mean current–voltage relationships of persistent I_{Na} expressed as percentage of peak I_{Na} for wild-type ($n = 30$), R853Q ($n = 21$), L1563V ($n = 14$), and R1882Q ($n = 25$). Dotted lines indicate zero current level. (*C*) Typical wild-type and mutant I_{Na} traces elicited at −25, −30, and −35 mV (*Upper*). Note the slower inactivation time course of R1882Q I_{Na} vs. wild-type (pink star). (*Lower*) Average fast time constants (τ_f) of I_{Na} inactivation plotted against test potential. (*Inset*) Boxed τ_f values on an expanded scale. R1882Q channels show larger τ_f values versus wild-type (see data with statistics in Table 2).

1,000-ms duration and an example trace of such an experiment is shown in Fig. 4*B*. The input–output relationships, representing the number of action potentials elicited by the corresponding current input in the axon initial segment (AIS) model cell are shown in Fig. 4*C*. In dynamic clamp experiments comparing the input–output curves it was readily apparent that each variant produced a unique profile. R1882Q had a left shift in the rheobase and achieved significantly higher action potential firing than wild-type or R853Q channels (Fig. 4 *C* and *D*). L1563V channels had a rheobase similar to wild-type but exhibited a markedly higher gain and could achieve a peak action potential firing rate similar to R1882Q. R853Q channels showed a significantly reduced action potential firing rate across a broad range of input currents beyond what might have been expected by visual inspection of voltage clamp data alone, highlighting the utility of the dynamic action potential-clamp approach in resolving the impact of multiple changes in biophysical properties.

Next, we used more biologically realistic stimuli to investigate the modulation of action potential firing activity by using the Ornstein–Uhlenbeck model of synaptic noise (Fig. 5 *A* and *B*). This form of stimulation differed from the step current in that it produced more random action potential firing intervals and achieved a lower overall frequency of firing more reminiscent of the type of behavior seen in real neurons. The overall pattern of the input–output relationships formed using synaptic stimulation versus step current was very similar, providing an additional validation of the variant behavior while allowing for additional parameters to be extracted from the analysis, such as interspike interval, V_m, and the ability to model the effect sustained V_m levels at different conductance states (23). In hybrid neurons incorporating either wild-type or mutant I_{Na}, we scaled the synaptic current using a set of excitatory (g_e) to inhibitory (g_i) conductance ratios and probed the input–output profile (Fig. 5 *C* and *D*). Increasing the g_e:g_i ratio from 1 to 3 produced gradual V_m depolarizations and high-amplitude V_m fluctuations of the model cell, typical for cortical neurons in vivo. Over a wide range of g_e:g_i ratios, the R853Q containing hybrid model exhibited significantly decreased action potential firing, whereas the R1882Q containing hybrid model showed a significantly increased action potential firing. Analysis of L1563V in the dynamic clamp showed a similar rheobase to wild-type and could achieve levels of action potential firing to that seen with R1882Q at higher levels of stimulation (Fig. 5 *C* and *D*). Inspection of the I_{Na} action currents showed how increasing g_e:g_i ratios decreased availability as reflected by the reduced peak I_{Na} during repetitive action potential firing. Detailed analysis of action potential waveforms was undertaken for wild-type or mutant channels (Fig. 5*E*), and the relationship of the g_e:g_i ratio of the stimulating current to steady-state V_m, action potential upstroke velocity (AP rise), action potential width, and the time constant of action potential decay are shown (Fig. 5*E*). Relative to wild-type, the AIS model cell incorporating R1882Q channels was more depolarized and exhibited wider action potentials that repolarized slower, whereas these features were unchanged in model cells incorporating R853Q or L1563V channels. As shown

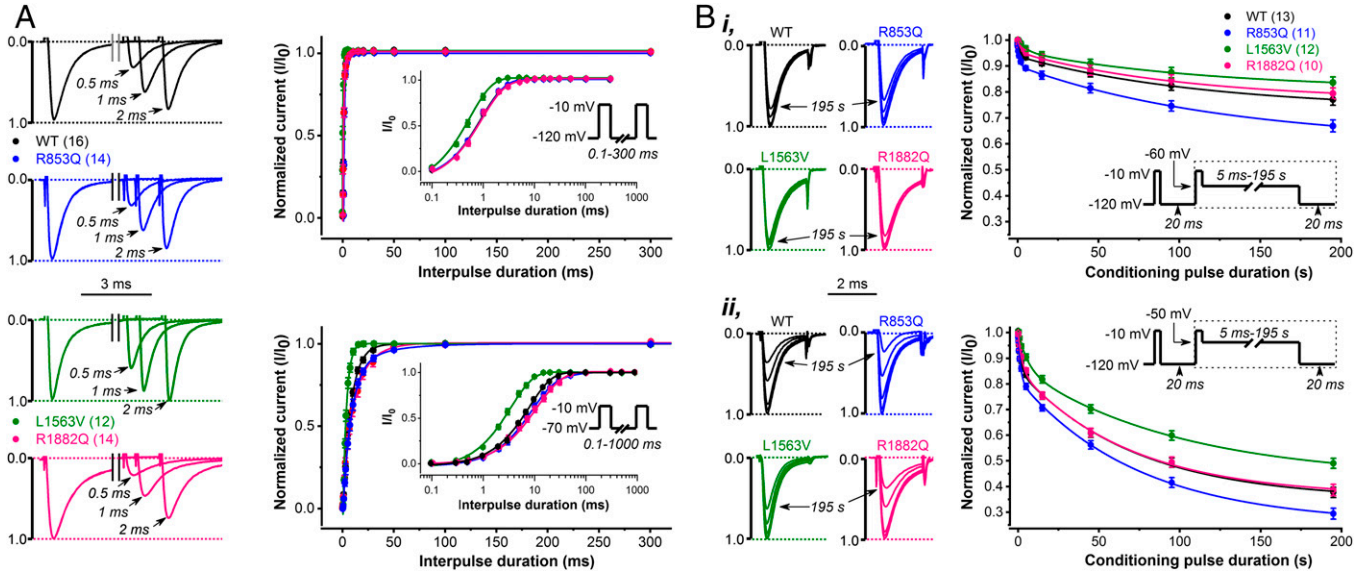

Fig. 3. Recovery from inactivation and development of slow inactivation in CHO cells expressing WT, R853Q, L1563V, or R1882Q $Na_v1.2$ channels. (*A*) Accelerated recovery of L1563V channels versus wild-type revealed with paired-pulse protocols of HP values of −120 or −70 mV, respectively. (*Left*) Representative P1 (control)- and P2-elicited traces elicited from a HP of −120 mV and using recovery interpulse intervals of 0.5, 1, and 2 ms. Plots (*Right*) show normalized wild-type and mutant peak I_{Na} as a function of interpulse duration. Note the effect of HP (*Upper*: −120 mV; *Lower*: −70 mV) on the time course of I_{Na} recovery. (*Insets*) Voltage protocols. (*B*) Enhanced slow inactivation for R853Q and reduced slow inactivation for L1563V versus wild-type channels. The extent of slow inactivation is indicated by the fractional reduction in peak I_{Na} during the 2-ms test pulse (P2) relative to that recorded in the first 2-ms prepulse (P1). At any P2, the fraction that enters slow inactivation equals 1 − P2/P1. (*Insets*) Voltage protocols with boxed areas representing the repeated voltage motif, including the time intervals of increasing duration. Note the effect of V_m on slow inactivation, −60 mV (*i*) versus −50 mV (*ii*), respectively. See data with statistics in Table 2.

with step current input, the BFNIS variant L1563V produced action potential firing that was similar to control for smaller g_e:g_i ratios (≤2.5) but departed significantly from wild-type for larger inputs (Fig. 5*D*).

Taken together, these unique dynamic clamp experiments provide a direct readout of the deleterious effects of $Na_v1.2$ mutations on model neuron excitability and unequivocally demonstrate the effect of loss-of-function and gain-of-function in the presence of R853Q and R1882Q channels, respectively. Interestingly, L1536V differed from R1882Q in that the increase in action potential firing only occurred at higher stimulus currents and impacted neuronal function less pervasively, thus providing an important clue as to why the BFNIS variant may be self-limiting, and also suggesting a mechanism-based therapeutic approach, such that drugs that reduce action potential firing at low stimulation currents could be effective in DEE patients with R1882Q or similar variation.

Discussion

SCN2A has emerged as a major gene implicated in neonatal-, infantile-, and even childhood-onset epilepsies, with a number of distinct epilepsy syndromes recently recognized (1, 2, 7). Many of these are also associated with cognitive and behavioral impairments that range in type and severity (12). Analyses of *SCN2A* mutations suggest a correlation between variant clinical presentation, functional impact, and pharmacosensitivity (7). Here we studied two of the most recurrent DEE mutations, R1882 with early-onset DEE and R853Q with infantile spasms. We undertook a clinical and biophysical analysis to explore the mechanisms underpinning the distinctive phenotypes produced by these variants and contrast these findings with L1563V associated with the self-limited syndrome of BFNIS.

The clinical features and treatment response in the newly identified and previously published patients with R853Q, R1882Q, and L1563V mutations are summarized in Table 1. R853Q and R1882Q result in DEE, whereas L1563V causes self-limited, pharmacoresponsive epilepsy. We confirm and expand upon a previous report (7) of distinct phenotypic segregation between R1882Q and R853Q cases suggesting that the biophysical consequences, unique to each variant, would be major determinants of clinical phenotype. The clinical presentations with these two mutations differ in seizure onset age and seizure type. Furthermore, there is emerging evidence of differences in the type of movement disorder (choreoathetosis in those with R853Q mutations), presenting symptom (seizures in R1882Q, developmental delay in R853Q), and pharmacosensitivity (discussed below).

To better understand the genotype–phenotype correlations due to *SCN2A* mutations, we complemented voltage clamp analysis, which models the biophysical consequences of a given variant, with dynamic clamp analysis, which more accurately predicts the contribution of $Na_v1.2$ channel mutations to neuronal excitability and the neurophysiological consequences of such variants. Results show unequivocally that the R1882Q variant leads to gain-of-function and increased neuronal excitability, whereas the R853Q variant results in loss-of-function and decreased neuronal excitability, and finally the L1563V mutation only produces an enhanced excitability profile in the presence of higher intensity stimuli.

The functional changes in R853Q channels, determined by voltage clamp analysis, include a negative shift of the steady-state inactivation and an enhanced entry into slow inactivation, suggesting a loss-of-function phenotype compared with wild-type channels. This observation was highlighted and strengthened by dynamic clamp analysis that showed a dramatic reduction in action potential firing across a range of input currents that was a far greater loss-of-function than that might be predicted by intuitive interpretation of voltage clamp data.

In voltage clamp experiments, R1882Q channels exhibited shifts in both activation and inactivation curves and slower fast inactivation. These changes, combined, underpin gain-of-function. In addition, disrupted inactivation can provide a causative mechanism for increased persistent I_{Na} (19, 24). Persistent I_{Na} can reduce the current needed to reach action potential threshold and supports subthreshold oscillations and repetitive action potential firing (25). Dynamic clamp experiments using realistic stimuli with R1882Q channels showed that the sum of all of the biophysical changes contributed to a more a depolarized V_m that could have significant impacts by further contributing to enhanced excitability.

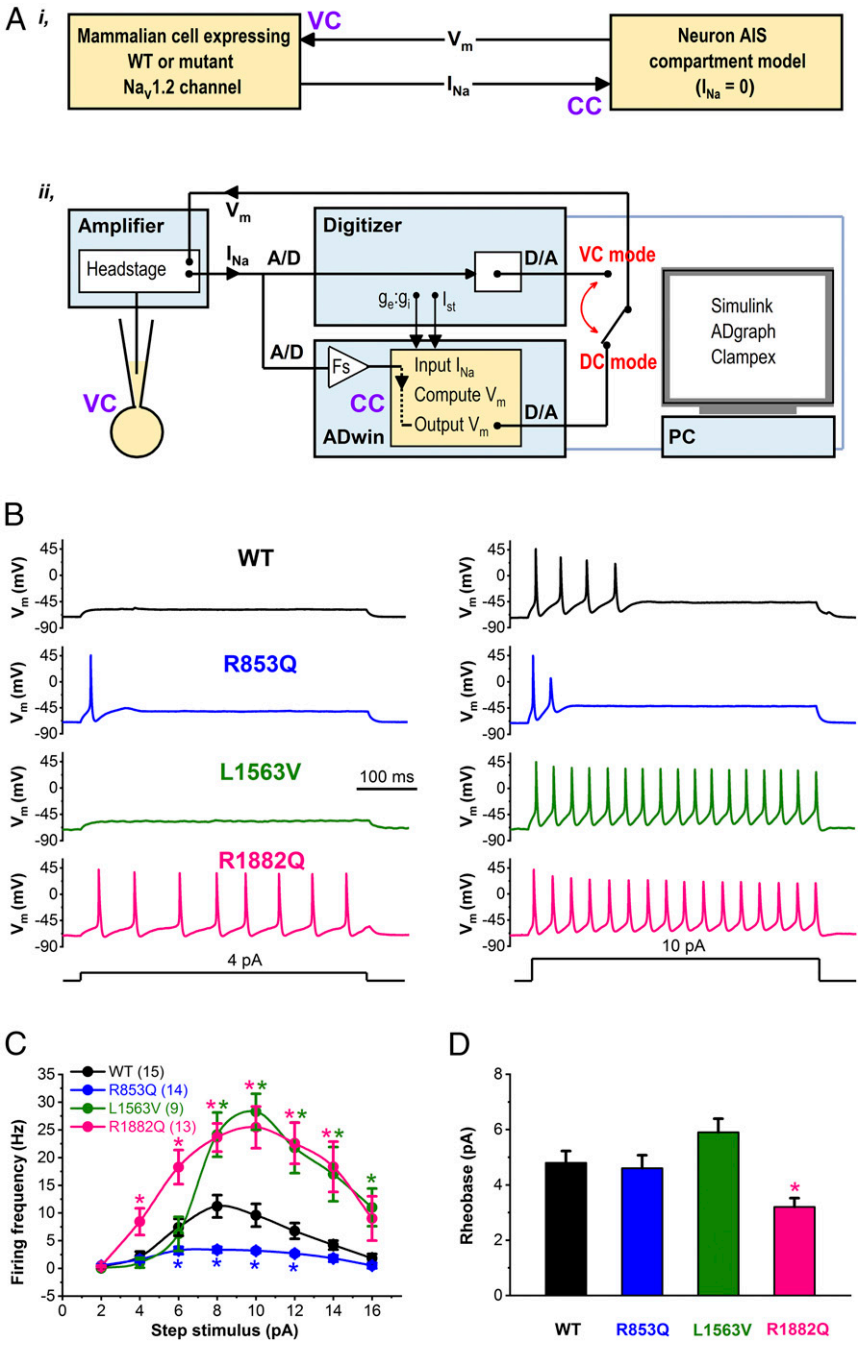

Fig. 4. Dynamic action potential-clamp experiment implementing WT, R853Q, L1563V, or R1882Q I_{Na}. (*A*, *i*) Schematic representation of the dynamic clamp technique used to effectively replace the in silico I_{Na} of the virtual AIS compartment model with I_{Na} expressed in a mammalian (CHO) cell. (*ii*) In dynamic clamp (DC) mode, I_{Na} is recorded from a CHO cell, digitized (A/D), scaled (*Fs*), and continuously applied to the virtual (model) cell as an external current input. The model cell is in current clamp (CC) mode and its V_m is computed in real-time by the PC-controlled ADwin system. The computed V_m is converted into an analog signal (D/A), sent back to the amplifier, and applied as a voltage clamp (VC) command to the CHO cell. Action potential firing in the model cell is triggered either by step stimulus currents (I_{st}) or synaptic current (g_e:g_i). The set-up enables switching between dynamic clamp and conventional voltage clamp modes. (*B*) Dynamic action potential-clamp experiments reveal Na$_V$1.2 channel gain-of-function or loss-of-function. Action potential firing with model cell incorporating wild-type, R853Q, L1563V, or R1882Q I_{Na} in response to increasing I_{st}, in the range between 0 and 16 pA, in 2-pA increments. Representative V_m changes elicited by 4- or 10-pA step currents are shown. (*C*) Input–output showing the I_{st} dependence of action potential firing. Data are mean ± SEM; *n*, number of experiments between parentheses; Note the altered action potential firing of the model cell in the presence of mutant I_{Na} compared with wild-type (*$P < 0.05$). (*D*) Rheobase (*$P < 0.05$, compared with wild-type); *n*, same as in *C*.

An increase in neuronal excitability was also seen with the L1563V channels, albeit only in the presence of a relatively high-stimulus strength, and to a lesser degree than the R1882Q channel. However, in dynamic clamp mode, a typical AIS model cell incorporating L1563V channels is capable of switching between normal activity and increased action potential firing modes when stimulus current strength increases above a critical magnitude. This functional profile would be impossible to intuit from voltage clamp analysis of the L1563V variant given the relatively small but opposing changes of the activation and inactivation curves and an enhanced recovery from fast inactivation compared with wild-type, highlighting a strength of the

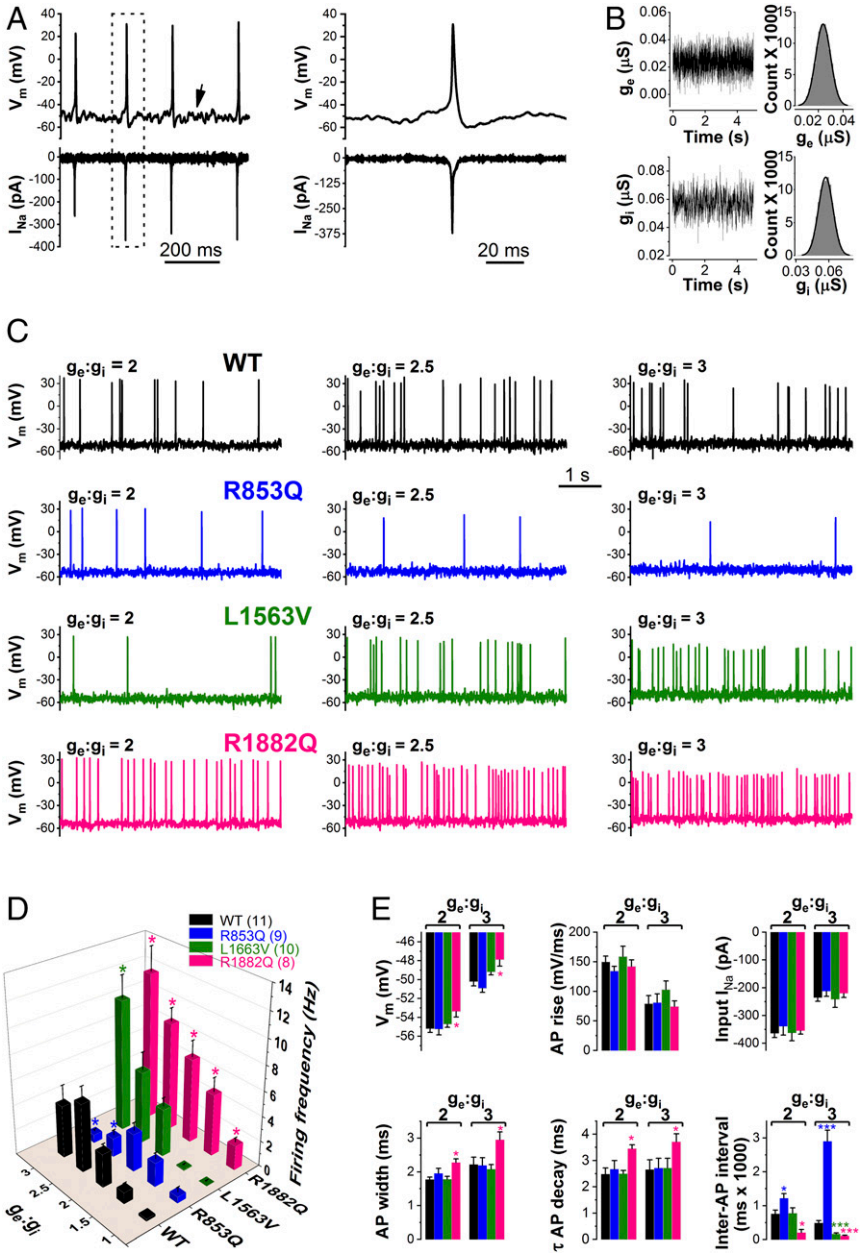

Fig. 5. Firing of the model cell incorporating WT, R853Q, L1563V, or R1882Q I_{Na} in response to synaptic conductance input. (*A*) Typical firing responses of the AIS model cell incorporating wild-type I_{Na}. The V_m changes (upward deflections) and associated scaled input I_{Na} (downward deflections) are shown. Note the V_m fluctuations typical for these types of experiments (arrow). (*Right*) Boxed action potential and I_{Na} on an expanded timescale. (*B*) Time course and magnitude of g_e (*Upper*) and g_i (*Lower*), respectively, with an excitatory and inhibitory (g_e:g_i) ratio value of 2. *Inset* histograms define mean g_e and g_i values of 0.0238 pA and 0.0571 pA, respectively. (*C*) Firing responses with g_e:g_i values of 2, 2.5, and 3, respectively. Note the change in firing frequencies because of $Na_v1.2$ channel loss-of-function (R853Q) or gain-of-function (L1563V, R1882Q). (*D*) Input–output relationships in the model cell as a function of g_e:g_i; *n*, number of experiments between parentheses; $*P < 0.05$, compared with wild-type. (*E*) Steady-state V_m, action potential (AP) upstroke velocity, input I_{Na} amplitude, AP width, time course (τ) of repolarization, and interspiking interval values, respectively, as a function of g_e:g_i. Data are mean ± SEM; $*P < 0.05$, $***P < 0.001$ compared with wild-type (one-way ANOVA); *n*, same as in *D*.

dynamic action potential-clamp method in providing meaningful frameworks for understanding variant functional mechanisms.

More complex aspects of AIS and *SCN2A* biology will also need to be considered in future studies. In future dynamic action potential clamp studies, the complexity of the virtual model can be increased by adding not only different and additional conductances but also adding somatic and dendritic compartments capable of mimicking more realistic morphology (26). In the cortex, $Na_v1.2$ is expressed in excitatory pyramidal cells (27) and somatostatin (SST)-expressing interneurons (28); the impacts of each type of mutation at a network level are not yet known. Previous studies in animal models show that the specific expression pattern and subcellular localization of $Na_v1.2$ channels in the AIS correlates with age and neuron type (29), implying that $Na_v1.2$ channel dysfunction may have the biggest effect on AIS function in infants (16). It has been proposed that loss of $Na_v1.2$ channel function due to de novo missense mutations is associated with autism spectrum disorder (10). However, our data demonstrate that $Na_v1.2$ channel mutations resulting in loss-of-function may also constitute a plausible cellular pathomechanism for later-onset DEE and that not

only gain-of-function mutations can lead to epilepsy syndromes, as previously suggested (10). The mechanism underlying the paradoxical observation that loss-of-function in $Na_v1.2$ can lead to infantile seizures and epilepsy is unknown and needs further studies.

In vivo, the V_m of cortical pyramidal neurons exhibits subthreshold fluctuations due to the spatiotemporal integration of excitatory and inhibitory inputs (30). In dynamic clamp experiments, action potential firing in the AIS compartment model could efficiently be initiated by depolarizing current steps or in response to scalable g_e:g_i input, mimicking a realistic synaptic environment (31). The specific functional changes in our dynamic clamp data may underpin the distinct phenotypes in infants with R1882Q and R853Q mutations. Further work will be required to confirm that other *SCN2A* mutations causing early-onset and later-onset DEE segregate gain-of-function and loss-of-function effects, respectively. Detailed understanding of molecular mechanisms in individuals with *SCN2A* DEE is needed to guide development of urgently needed precision medicine approaches. For this, channel dysfunction and the likely associated cellular pathomechanisms will need to be coinvestigated.

So far, the relationship between functional effect of the *SCN2A* mutation and response to sodium-channel blockers remains incompletely understood. There have been no clinical trials of these drugs in *SCN2A*-associated epilepsies. As may be expected with a gain-of-function mutation, some patients with R1882Q mutations become seizure-free with phenytoin. However, improvement with phenytoin was not universal and other sodium-channel blockers were less effective. It is perhaps not surprising that reduction of seizures with drugs seen in some patients with DEE fail to improve development as the cellular and network-scale impacts of the *SCN2A* mutation are likely to extend beyond epileptogenesis into cognitive and movement functions and highlighting the need for more specific mechanisms that fundamentally modify disease progression and address seizures and comorbidities (12). Given the loss-of-function impact the R853Q variant would have on neurons, it is perhaps not surprising that sodium-channel blockers are usually contraindicated. Infantile spasms and subsequent epilepsy may emerge as a secondary consequence of altered neuronal firing in R853Q patients, further complicating the use of sodium-channel blockers as they could be beneficial to reducing seizures but may paradoxically exacerbate the underlying loss-of-function in sodium-channel activity. This is reflected in clinical observations of both seizure exacerbation and benefit in different patients, yet in one patient cessation of treatment led to an overall improvement in function, despite seizures returning, and suggesting that sodium-channel blockers may provide no net benefit in those with R853Q mutations. Further study of the effects of sodium-channel blockers in both groups is required, including considering differential effects of different drugs, high and low drug doses, and impacts at different ages on different seizure types and development. The differential functional and phenotypic effects of the *SCN2A* mutations suggest that novel treatments will need to be tailored to the functional impacts of the mutation; it is unlikely that a single-treatment strategy for all *SCN2A*-associated disorders will be effective.

Dynamic clamp analysis provides clear benefits over voltage clamp analysis. The output is in the interpretation-friendly format of action potential firing, without the need to intuitively or computationally interpret voltage clamp recordings and with significantly less burden on experimenter time, with a day or two of dynamic clamp recording providing a definitive analysis of variant impact on excitability versus weeks of voltage clamp analysis. In our experiments, heterologous expression of the α-subunit alone was sufficient for generating functional $Na_v1.2$ channels, although the lack of β-subunit and the heterologous channel environment may have affected $Na_v1.2$ channel function in the hybrid neuron, as it would for traditional voltage clamp studies. Limitations of the dynamic action potential-clamp technique, such as the reliance on the mathematical description of model cell ionic currents, or issues relating to the scaling of the implemented ionic current, have been reviewed elsewhere (32). In CHO cells, I_{Na} densities of R853Q channels were smaller, whereas those of R1882Q channels were larger compared with wild-type (Fig. 1). In dynamic action potential-clamp experiments, downscaling of the R853Q input I_{Na} exacerbated loss-of-function, whereas the upscaling of the input R1882Q I_{Na} exacerbated gain-of-function (*SI Appendix*, Figs. S7 and S8). However, it is uncertain to what extent the heterologous expression of $Na_v1.2$ channel variants in mammalian cells can replicate the true expression levels of the variants in neuronal membranes.

Dynamic clamp is well positioned as a rapid diagnostic and will supplant voltage clamp analysis for modeling of voltage-gated ion channels. Further developments of real-time models that incorporate heterosynaptic modeling of ligand-gated channels (33) could offer a broader impact of this approach in epilepsy and other neurogenetic diseases. With advances in real-time computation platforms, the ability to implement more complex in silico models enhances our ability to evaluate the impact of variants in different brain networks for separable prediction of effects on cognition, movement, and other functions, such as respiration and cardiac control that may impact sudden unexpected death in epilepsy and other comorbidities seen in epilepsy. A recent study shows how inexpensive it is to add a dynamic clamp on every rig (34). Dynamic clamp is well positioned to impact drug discovery by providing a disease-state relevant model that should allow a more predictive link to clinical effect than currently used voltage clamp assays, while exploiting the same biological and instrumentation resources.

Materials and Methods

Patients. All patients, or their parents or legal guardian in the case of minors or individuals with intellectual disability, gave written informed consent. The study was approved by the Human Research Ethics Committee of Austin Health, Melbourne. Nineteen individuals with the R1882Q or R853Q *SCN2A* mutations were identified from the literature, and from an *SCN2A* support group (www.scn2a.org). Clinical data collection and analysis is described in *SI Appendix*.

Plasmids, Cell Culture, and Transfection. For details on plasmid construction, CHO cell culture, transfection procedures, and electrophysiological recordings, see the expanded materials and methods used described in *SI Appendix*.

Voltage Clamp Experiments and Curve Fitting. Depolarization-activated whole-cell sodium currents (I_{Na}) from CHO cells transiently expressing wild-type or mutant $Na_v1.2$ channels were recorded using an Axopatch 200B amplifier (Molecular Devices) controlled by a pCLAMP 9/DigiData 1440 acquisition system (Molecular Devices). Experiments were performed at room temperature (23 ± 0.5 °C). Currents and potentials were low-pass–filtered at 10 kHz and digitized at 50 kHz. Data were analyzed off-line using Clampfit 9.2 (Molecular Devices) and Origin 9.0 (Microcal Software).

The current-voltage (*I–V*) relationships, and I_{Na} kinetics were determined by voltage clamp protocols, as diagrammed in Figs. 1–3 and detailed in *SI Appendix*.

Dynamic Action Potential Clamp. Our approach is based on the dynamic action potential-clamp technique (13, 14), where heterologously expressed wild-type or mutant Nav1.2 channels currents are incorporated into a biophysically realistic model of the distal AIS compartment of a cortical pyramidal neuron (35). In most neurons, this compartment contains the site of action potential initiation and plays a major role in in action potential firing dysfunction in epileptogenesis (29). The compartment model was built in Simulink (Mathworks) and it contains $Na_v1.6$ channel sodium current ($I_{Nav1.6}$), fast rectifying potassium current (I_{Kv}), synaptic current (I_{syn}), passive leak current (I_{pas}), and membrane capacitance (C_m). The Simulink model of the AIS compartment and the nested models of I_{Kv}, I_{pas}, I_{syn}, and $I_{Nav1.6}$ are shown in *SI Appendix*. The parameters of the various conductances implemented in our model were set for performance at room temperature (23 °C), consistent with experimental conditions for recording $Na_v1.2$ channel I_{Na} in CHO cells. As shown in Fig. 4*A*, the virtual cell is in current-clamp mode, whereas the real CHO cell is in voltage clamp mode. The command potential for the CHO cell is the V_m of the virtual cell and the wild-type or mutant I_{Na} elicited in the transfected CHO cell serves as input current that replaces the original I_{Na} of the virtual cell. The Simulink model is converted into C library using Matlab Real-Time Workshop, compiled and simulated using a 40-bit ADwin-Pro II processing unit (Jäger Computergesteuerte Messtechnik) equipped with a TigerSHARC ADSP-TS101S processor (Analog Devices) with 300-MHz clock rate, 768-kB local memory, and 256 MB RAM. The processor provides support of fixed and floating-point data types and enables computationally intensive real-time computing with precision and high speed

(140 kHz). At each iteration, the instantaneous V_m is calculated by solving the Hodgkin–Huxley equations of the AIS neuronal model (36) in conjunction with the stimulus current (I_{st}) and the scaled wild-type or mutant I_{Na} (input I_{Na}) from the CHO cell. The computed V_m is sent back to the Axopatch 200B amplifier (Molecular Devices) as an analog command signal. As a result, the studied channel's conductance directly interacts with the virtual cell's V_m and its contribution to the action potential is revealed in real-time. Data are stored as FIFO arrays in ADwin memory and can be monitored in real-time using ADgraph software provided with the ADwin package.

To increase the flexibility of the model, the variable parameters (e.g., peak conductance and reversal potential for different ion-channels) can be modified as input arguments in ADbasic, the programming language of the ADwin system. Parameter setting in ADwin and data are automatically saved on a hard disk for further analysis. Subthreshold voltage responses or firing of the AIS model were elicited by using two methods, consisting of either a 0- to 30-pA step current injections in 2-pA increments commanded via the Clampex module of pCLAMP 9 software or enabling synaptic current input generating directly within the ADwin-Pro II processing unit and input to the in silico model. To approximate synaptic background activity, we adapted a stochastic model that exploits the Ornstein–Uhlenbeck process and generates synaptic current as a sum of two independent excitatory and inhibitory synaptic conductances (g_e and g_i, respectively), as previously described (31, 37). Various g_e:g_i ratios were set by scaling the mean and SD of g_e and keeping g_i unchanged. Typically, the V_m of our model produced constant fluctuations (Fig. 5*A*) and the average resting V_m (around −70 mV) exhibited more depolarized mean values with increasing g_e:g_i ratios (Fig. 5 *C* and *E*). The latter method represents a more realistic approximation of realistic postsynaptic signaling. Ionic currents in the virtual cell in combination with wild-type I_{Na} from the CHO cell result in control activity (action potential firing), whereas mutant I_{Na} results in activity that mimics excitatory neuron behavior in a patient from which the mutant channel was derived. Before undertaking dynamic clamp experiments, the background (endogenous) current ($I_{background}$), present in the voltage-clamped CHO cell is estimated and subtracted using the linear leak subtraction control of the Axopatch 200B amplifier. In all dynamic clamp experiments, the heterologously expressed wild-type or mutant I_{Na} recorded in the CHO cell is multiplied by a scale factor (F_s). To assign the F_s value for the I_{Na}, the peak I_{Na} amplitude is first determined in voltage clamp mode by recording current–voltage relationships elicited from HP values of −120 and −70 mV. Then, in dynamic clamp mode, the I_{Na} amplitude is scaled to a magnitude value similar to the original model cell's sodium current amplitude (~350 pA). I_{Na} is typically downscaled (approximately 10- to 15-fold), thus $I_{background}$ contribution to the experiment can be considered as negligible. We did not adjust for possible differences between wild-type and mutant I_{Na} densities expressed in CHO cells, thus differences in action potential firing are mainly attributed to the altered biophysical properties of the given $Na_v1.2$ channel variant. In all dynamic clamp experiments, the nonscaled and scaled input I_{Na}, the stimulus waveform, the V_m, and the total synaptic current in the model cell were simultaneously recorded. We systematically evaluated the model cell's robustness by scaling the C_m and/or the various conductances in the AIS compartment, and analyzing the interaction between the passive and/or the active model features in the presence of external wild-type or mutant $Na_v1.2$ channel I_{Na} (*SI Appendix*, Figs. S2–S9). The analysis of input I_{Na} and action potential parameters is presented in the *SI Appendix*.

Statistical Analysis. Data are presented as mean ± SEM; *n*, number of experiments. Statistical comparison between more than two groups was performed using one-way ANOVA followed by Bonferroni post hoc test. Two-way repeated-measures ANOVA followed by the Holm–Sidak post hoc test was used for comparing the $Na_v1.2$ channel variants and the different firing frequencies. Statistical significance is defined by $P < 0.05$.

ACKNOWLEDGMENTS. We thank the patients and their families for participating in our research; and Ian C. Forster for helpful comments on an earlier version of this manuscript. This study was supported by Australian Research Council Centre of Excellence for Integrative Brain Function Grant CE14010007; National Health and Medical Research Council (NHMRC) programme Grant 10915693 and NHMRC Fellowship GNT1005050 (to S.P.); and a Practitioner fellowship (to I.E.S.). K.B.H. was supported by a clinician-scientist fellowship from the Murdoch Childrens Research Institute. G.B. was funded by RogCon, Inc. The Florey Institute of Neuroscience and Mental Health is supported by Victorian State Government infrastructure funds.

1. Heron SE, et al. (2002) Sodium-channel defects in benign familial neonatal-infantile seizures. *Lancet* 360:851–852.
2. Howell KB, et al. (2015) *SCN2A* encephalopathy: A major cause of epilepsy of infancy with migrating focal seizures. *Neurology* 85:958–966.
3. Mantegazza M, Curia G, Biagini G, Ragsdale DS, Avoli M (2010) Voltage-gated sodium channels as therapeutic targets in epilepsy and other neurological disorders. *Lancet Neurol* 9:413–424.
4. Allen AS, et al.; Epi4K Consortium; Epilepsy Phenome/Genome Project (2013) De novo mutations in epileptic encephalopathies. *Nature* 501:217–221.
5. Carvill GL, et al. (2013) Targeted resequencing in epileptic encephalopathies identifies de novo mutations in *CHD2* and *SYNGAP1*. *Nat Genet* 45:825–830.
6. Stessman HA, et al. (2017) Targeted sequencing identifies 91 neurodevelopmental-disorder risk genes with autism and developmental-disability biases. *Nat Genet* 49: 515–526.
7. Wolff M, et al. (2017) Genetic and phenotypic heterogeneity suggest therapeutic implications in *SCN2A*-related disorders. *Brain* 140:1316–1336.
8. Nakamura K, et al. (2013) Clinical spectrum of *SCN2A* mutations expanding to Ohtahara syndrome. *Neurology* 81:992–998.
9. Neale BM, et al. (2012) Patterns and rates of exonic de novo mutations in autism spectrum disorders. *Nature* 485:242–245.
10. Ben-Shalom R, et al. (2017) Opposing effects on $Na_V1.2$ function underlie differences between SCN2A variants observed in individuals with autism spectrum disorder or infantile seizures. *Biol Psychiatry* 82:224–232.
11. Fromer M, et al. (2014) De novo mutations in schizophrenia implicate synaptic networks. *Nature* 506:179–184.
12. Scheffer IE, et al. (2017) ILAE classification of the epilepsies: Position paper of the ILAE Commission for Classification and Terminology. *Epilepsia* 58:512–521.
13. Berecki G, et al. (2006) Long-QT syndrome-related sodium channel mutations probed by the dynamic action potential clamp technique. *J Physiol* 570:237–250.
14. Berecki G, et al. (2005) *HERG* channel (dys)function revealed by dynamic action potential clamp technique. *Biophys J* 88:566–578.
15. Misra SN, Kahlig KM, George AL, Jr (2008) Impaired $Na_V1.2$ function and reduced cell surface expression in benign familial neonatal-infantile seizures. *Epilepsia* 49: 1535–1545.
16. Xu R, et al. (2007) A childhood epilepsy mutation reveals a role for developmentally regulated splicing of a sodium channel. *Mol Cell Neurosci* 35:292–301.
17. Scalmani P, et al. (2006) Effects in neocortical neurons of mutations of the $Na_{(v)}1.2$ Na^+ channel causing benign familial neonatal-infantile seizures. *J Neurosci* 26: 10100–10109.
18. Taddese A, Bean BP (2002) Subthreshold sodium current from rapidly inactivating sodium channels drives spontaneous firing of tuberomammillary neurons. *Neuron* 33: 587–600.
19. Chadda KR, Jeevaratnam K, Lei M, Huang CL (2017) Sodium channel biophysics, late sodium current and genetic arrhythmic syndromes. *Pflugers Arch* 469:629–641.
20. Sokolov S, Scheuer T, Catterall WA (2007) Gating pore current in an inherited ion channelopathy. *Nature* 446:76–78.
21. Kuo CC, Bean BP (1994) Na^+ channels must deactivate to recover from inactivation. *Neuron* 12:819–829.
22. Cohen CJ, Bean BP, Tsien RW (1984) Maximal upstroke velocity as an index of available sodium conductance. Comparison of maximal upstroke velocity and voltage clamp measurements of sodium current in rabbit Purkinje fibers. *Circ Res* 54:636–651.
23. Armstrong CM (2006) Na channel inactivation from open and closed states. *Proc Natl Acad Sci USA* 103:17991–17996.
24. Motoike HK, et al. (2004) The Na^+ channel inactivation gate is a molecular complex: A novel role of the COOH-terminal domain. *J Gen Physiol* 123:155–165.
25. Vanoye CG, Lossin C, Rhodes TH, George AL, Jr (2006) Single-channel properties of human $Na_V1.1$ and mechanism of channel dysfunction in *SCN1A*-associated epilepsy. *J Gen Physiol* 127:1–14.
26. Yu Y, Shu Y, McCormick DA (2008) Cortical action potential backpropagation explains spike threshold variability and rapid-onset kinetics. *J Neurosci* 28:7260–7272.
27. Lorincz A, Nusser Z (2008) Cell-type-dependent molecular composition of the axon initial segment. *J Neurosci* 28:14329–14340.
28. Li T, et al. (2014) Action potential initiation in neocortical inhibitory interneurons. *PLoS Biol* 12:e1001944.
29. Wimmer VC, Reid CA, So EY, Berkovic SF, Petrou S (2010) Axon initial segment dysfunction in epilepsy. *J Physiol* 588:1829–1840.
30. Petersen CCH (2017) Whole-cell recording of neuronal membrane potential during behavior. *Neuron* 95:1266–1281.
31. Destexhe A, Rudolph M, Fellous JM, Sejnowski TJ (2001) Fluctuating synaptic conductances recreate in vivo-like activity in neocortical neurons. *Neuroscience* 107: 13–24.
32. Wilders R (2006) Dynamic clamp: A powerful tool in cardiac electrophysiology. *J Physiol* 576:349–359.
33. Dixon CL, Zhang Y, Lynch JW (2015) Generation of functional inhibitory synapses incorporating defined combinations of $GABA_A$ or glycine receptor subunits. *Front Mol Neurosci* 8:80.
34. Desai NS, Gray R, Johnston D (2017) A dynamic clamp on every rig. *eNeuro* 4: ENEURO.0250-17.2017.
35. Hu W, et al. (2009) Distinct contributions of $Na_{(v)}1.6$ and $Na_{(v)}1.2$ in action potential initiation and backpropagation. *Nat Neurosci* 12:996–1002.
36. Hodgkin AL, Huxley AF (1952) A quantitative description of membrane current and its application to conduction and excitation in nerve. *J Physiol* 117:500–544.
37. Destexhe A, Rudolph M, Paré D (2003) The high-conductance state of neocortical neurons in vivo. *Nat Rev Neurosci* 4:739–751.